JACS
JOURNAL OF THE AMERICAN CHEMICAL SOCIETY
Article
pubs.acs.org/JACS

# Unraveling the Mechanisms of Nonradiative Deactivation in Model Peptides Following Photoexcitation of a Phenylalanine Residue

Momir Mališ,[§,‡] Yohan Loquais,[⊥,∥,‡] Eric Gloaguen,[∥,⊥] Himansu S. Biswal,[⊥,∥,†] François Piuzzi,[⊥,∥] Benjamin Tardivel,[⊥,∥] Valérie Brenner,[⊥,∥] Michel Broquier,[▽,#] Christophe Jouvet,[▽,#,∞] Michel Mons,*[,⊥,∥] Nađa Došlić,[§] and Ivan Ljubić*[,§]

[§]Division of Physical Chemistry, Ruđer Bošković Institute, Bijenička cesta 54, HR-10002 Zagreb, Croatia
[⊥]CEA, IRAMIS, SPAM, Lab. Francis Perrin, URA 2453, CEA-Saclay, Bât 522, Gif-sur-Yvette, F-91191, France
[∥]CNRS, INC & INP, Lab. Francis Perrin, URA 2453, CEA-Saclay, Bât 522, Gif-sur-Yvette, F-91191, France
[▽]Université Paris-Sud 11, CLUPS / CNRS, LUMAT FR 2764, Bât 106, Orsay, F-91405, France
[#]CNRS, Université Paris-Sud 11, ISMO, UMR 8624, Bât 210, Orsay, F-91405, France

Supporting Information

**ABSTRACT:** The mechanisms of nonradiative deactivation of a phenylalanine residue after near-UV photoexcitation have been investigated in an isolated peptide chain model (*N*-acetylphenylalaninylamide, NAPA) both experimentally and theoretically. Lifetime measurements at the origin of the first $\pi\pi^*$ state of jet-cooled NAPA molecules have shown that (i) among the three most stable conformers of the molecule, the folded conformer NAPA B is ∼50-times shorter lived than the extended major conformer NAPA A and (ii) this lifetime is virtually insensitive to deuteration at the $NH_2$ and NH sites. Concurrent time-dependent density functional theory (TDDFT) based nonadiabatic dynamics simulations in the full dimensionality, carried out for the NAPA B conformer, provided direct insights on novel classes of ultrafast deactivation mechanisms, proceeding through several conical intersections and leading *in fine* to the ground state. These mechanisms are found to be triggered either (i) by a stretch of the $N_{Phe}H$ bond, which leads to an H-transfer to the ring, or (ii) by specific backbone amide distortions. The potential energy surfaces of the NAPA conformers along these critical pathways have been characterized more accurately using the coupled cluster doubles (CC2) method and shown to exhibit barriers that can be overcome with moderate excess energies. These results analyzed in the light of the experimental findings enabled us to assign the short lifetime of NAPA B conformer to a number of easily accessible exit channels from the initial $\pi\pi^*$ surface, most importantly the one involving a transfer of electronic excitation to an $n\pi^*$ surface, induced by distortions of the backbone peptide bond.

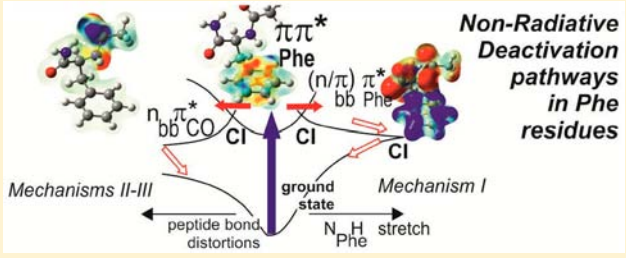


## 1. INTRODUCTION

The existence of nonradiative deactivations (NRD) in electronically excited proteins is of paramount importance for the stability of one of the major constituents of the living matter.[1−3] Progress toward understanding of these photochemical pathways is most readily made through studying small model peptides, as protein building blocks.[2,4−19] The multifaceted photochemistry of peptides is mainly due to the valence transitions involving three groups of chromophores:[20] the aromatic side chains of phenylalanine, tryptophan, tyrosine, and histidine, as well as terminal amino and carboxyl groups and the peptide bonds. The latter have long been recognized as a possible source for phenomena like fluorescence quenching.[4,6,7,21−27] In this context, model peptides containing aromatic amino acids and having modified, protected termini, such as *N*-acetylphenylalaninylamide (NAPA) and *N*-acetyltryptophanylmethylamide (NATMA), are considered invaluable because they retain complete peptide bonds, which qualifies them as protein chain model species.[5,11,22,28−37]

In the condensed phase, investigations on these systems are hampered by the coexistence of multiple conformers and by solvent and temperature effects, which make difficult a synergy between experiment and theory. On the other hand, from the seminal work by Levy et al.[29,38,39] gas phase experiments have been shown to be an extremely rich and accurate approach to the dynamical processes taking place in the excited state of neutral or charged peptides.[11,13−15,17,18,32] In particular, the short-lived excited states of protonated species with a tryptophan chromophore have been intensively documented through the use of ultrafast femtosecond lasers.[11,13,14] One of the important assets of the gas phase approach is the possible control of the peptide conformation (at least as long as nanosecond or picosecond lasers are used), which provides a doorway to conformation-selective effects[18,38] and enables

**Received:** June 6, 2012
**Published:** November 20, 2012



dx.doi.org/10.1021/ja3054942 | J. Am. Chem. Soc. 2012, 134, 20340−20351

elegant documentation of the relationship between structure and reactivity.

Along with these experimental advances, increasingly sophisticated theoretical methods have been developed allowing a detailed, high-level, point-to-point exploration of excited state potential energy surfaces (PES) of small to medium size molecular systems.[40] This in turn enables pinpointing conical intersections (CIs) between ground and excited state PESs providing an educated guess for the NRD reaction coordinate.[41] Such an approach was already used for peptide systems.[8,9,16,17,19,42−47] One notable NRD mechanism in excited neutral species was put forward by Shemesh et al. for NATMA[44] as well as Trp-Gly[46] and some other dipeptides[43,45] possessing the phenylalanine chromophore. This mechanism is highly specific however because it critically depends on the existence of the strong hydrogen bond connecting two neighboring peptide groups in the so-called $\gamma$-turn conformers (Figure 1). Along this H-bond, the H atom is transferred from the donor amine N to the acceptor carbonyl O atom providing a possible NRD pathway.

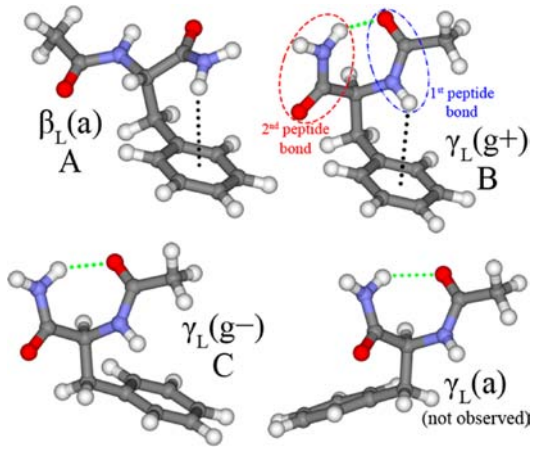


**Figure 1.** Four most stable conformers of NAPA, together with their assignment to the experimentally observed conformers (A−C). The relative energies of the $\beta_L$(a), $\gamma_L$(g+), $\gamma_L$(g−), and $\gamma_L$(a) conformers corrected for the harmonic zero-point energy are 0.00, 0.38, 1.01, and 1.42 kcal mol$^{-1}$, respectively, at the MP2/6-311+G(2d,p) level. They are found to be the most stable forms when the dispersive interactions are taken into account.[37,50] The extended backbone form is the most stable one (A); the two others are folded, with an intramolecular $C_7$ H-bond (green dots), with (B) or without (C) an additionally stabilizing NH−$\pi$ H-bond (black dots) between the $N_{Phe}H$ bond and the phenyl ring. Labels a and g± refer to the orientation of the Phe side chain relative to the backbone.

One promising way of looking for alternative NRD pathways is to turn to a full-dimensional nonadiabatic dynamics simulation[48] based on an efficient electronic structure method to provide qualitative hints about possible reaction coordinates leading to CIs. These can then be reinvestigated at a higher, more reliable level of theory. Such a procedure is likely to indicate a number of NRD pathways of general conceptual validity that could be suggestive of analogous protective photochemical mechanisms operative in proteins.[41] Apart from an excited state dynamics of microsolvated protonated tryptophan,[47] we are not aware of any previous similarly extensive dynamics study of a small model peptide, so we expect to see many other stones as yet left unturned.

The current work presents a combined experimental and theoretical approach to the excited state dynamics of the NAPA model peptide, based on the phenylalanine chromophore. The limited size of the phenyl group and its relatively well-resolved excited state spectroscopy make it an ideal starting candidate for probing the gas-phase photochemistry of the small protected peptides.[37] The experimental work takes advantage of the presence in a supersonic expansion of three conformers having different environments for the phenylalanine ring (see Figure 1).[33,49,50] Their excited state lifetimes were formerly investigated by laser-induced fluorescence, measured on the origin band of the $S_1 \leftarrow S_0$ first $\pi\pi^*$ transition, around ca. 266 nm. Two conformers, the so-called A and C species, were reported to be long-lived with lifetimes of 62 and 42 ns, respectively;[50] no fluorescence of the third species (B, assigned to the folded $\gamma$(g+) form, see Figure 1) could be detected, however, presumably because of a much shorter lifetime, suggesting a strongly conformer-selective deactivation process. A similar behavior was also reported for the fluorescence of the conformers of the phenylalanine amino acid[51,52] and tentatively assigned to a conformer-selective NRD via either intersystem crossing[51] (ISC) or vibronic coupling[52] between $\pi\pi^*$ and n$\pi^*$ states. In this case, however, the short lifetimes were found in the 20−30 ns range, that is, at least one order of magnitude larger than in the short-lived NAPA conformer. This motivated us to investigate the excited state lifetime of conformer B of NAPA in a pump−probe experiment at a picosecond resolution. The effect of selective deuterations on the excited state lifetime was also systematically investigated in a R2PI pump−probe experiment carried out at nanosecond resolution.

Simultaneously we have embarked upon theoretical efforts to build upon our previous study of NAPA conformers.[37] To this end, we carried out full-dimensional nonadiabatic (NA) dynamics simulations based on time-dependent density functional theory (TDDFT)[53−59] for the NAPA B conformer assuming a vertical photoexcitation. For the four lowest energy conformers, the observed species A, B, and C and the unobserved conformer $\gamma_L$(a), the pathways suggested by the NA dynamics were assessed at the more accurate coupled cluster doubles (CC2) level of theory. These results analyzed in the light of the experimental findings lead us to propose that the short lifetime of the NAPA B conformer is due to new NRD mechanisms, the majority of which are energetically more favorable and especially more universal than the one proposed previously.[43,45]

## 2. METHODOLOGY

**2.1. Experiment.** Isolated conformations of NAPA were formed and cooled to ∼10 K in a supersonic expansion after laser desorption of the NAPA sample (pellet made from a pressed mixture of graphite and NAPA powders) in a molecular beam machine described elsewhere.[60] The UV spectra were recorded, either by resonant two-photon ionization (R2PI) combined with time-of-flight (TOF) mass spectrometry or by laser-induced fluorescence (LIF), that is, by collecting the ions formed or the photons emitted as a function of a frequency-doubled nanosecond dye laser.

The combined use of mass spectrometry together with the spectral resolution achieved in a supersonic expansion also enabled us to probe selectively the deuterated isotopologues of NAPA, despite their coexistence in the sample. Since UV spectroscopy is sensitive to deuteration (in particular, through the zero point vibrational energy of these species), transitions of isotopomers (having the same isotopic content but deuterated on different sites) can be separated in principle. In particular, the isotopomers of the B form that differ by the position


dx.doi.org/10.1021/ja3054942 | J. Am. Chem. Soc. 2012, 134, 20340−20351

of the deuteron(s) on NH or on $NH_2$ can be easily distinguished: their UV spectral signatures have been unambiguously identified by IR/UV double resonance spectroscopy,[60] in combination with a mass-selected R2PI detection, which enabled us to provide isotopomer-selective IR spectra (see details in the Supporting Information).

Pump−probe experiments in the nanosecond regime were obtained with two frequency-doubled dye lasers pumped by a Nd:YAG and an excimer laser, whose time delay was electronically controlled. In the picosecond regime, the same laser-desorption source was adapted to a molecular beam setup having a TOF ion detection and benefiting synchronized picosecond lasers (fwhm time profile of 30 ps). Pump−probe experiments were carried out by collecting the ion signal with a delay control achieved using a computer-controlled optical delay line.[60] However, in this case, the laser bandwidth (~15 $cm^{-1}$) allowed us to achieve the spectral selectivity needed only for the B conformer of NAPA-$d_0$. Further experimental details are provided in the Supporting Information.

**2.2. Computational Methods.** The primary goal of the calculations is to account for the deactivation process of the NAPA molecule and in particular its first step, that is, the nonradiative transition undergone by the photoexcited $S_1$ state. Intersystem crossing should be considered a priori since it is indeed at play in toluene[61,62] and other alkylbenzenes,[63,64] being responsible, for example, for the shortened lifetime of toluene (86.4 ns at the origin[65]) compared with the radiative lifetime, estimated to be ~250 ns.[61,62] ISC, however, is likely not to be responsible for the much shorter lifetime (by a factor of 50) of the NAPA B conformer compared with the other species (see Supporting Information, Appendix S4 for a detailed discussion). The first step of deactivation should rather be assigned to an internal conversion, that is, nonradiative transition between singlet states. For this reason, triplet states have not been considered in the calculations, neither in the first step nor in the subsequent steps, even if, in this latter case, indirect evidence for the small population of triplet states has been given in phenylalanine-related molecules.[66]

*2.2.1. Nonadiabatic Dynamics with Tully's Surface Hopping.* The NA simulations of photodynamics in NAPA were performed within the framework of TDDFT.[53−59] We follow the methodological approach proposed by Mitrić et al.,[59] which combines localized Gaussian basis sets and Tully's surface hopping procedure.[67] The required inputs for the NA-TDDFT dynamics include ground and excited state analytical forces on the nuclei to determine their classical motion, as well as the matrix of nonadiabatic couplings, $D_{IJ}$, between the different adiabatic states $\Psi_J(\mathbf{r};\mathbf{R}(t))$ ($J$ = 1, ..., $N$):

$$D_{IJ} \equiv \left\langle \Psi_I(\mathbf{r};\,\mathbf{R}(t)) \middle| \frac{\partial \Psi_J(\mathbf{r};\,\mathbf{R}(t))}{\partial t} \right\rangle \tag{1}$$

Following Tavernelli et al.,[55−58] a set of auxiliary many-electron wave functions is introduced as an expansion in spin-adapted single-excitation configurations (CIS) built from the occupied ($i$) and virtual ($a$) set of the Kohn−Sham (KS) spin orbitals

$$|\Psi_J(\mathbf{r};\,\mathbf{R}(t))\rangle = \sum_{i,a} c_{i,a}^{J} \frac{1}{\sqrt{2}} (|\Phi_{i\alpha}^{a\beta}(\mathbf{r};\,\mathbf{R}(t))\rangle + |\Phi_{i\beta}^{a\alpha}(\mathbf{r};\,\mathbf{R}(t))\rangle) \tag{2}$$

which enables the calculation of nonadiabatic couplings in the framework of TDDFT. The calculation of the nonadiabatic coupling terms is thus reduced to the computationally intensive evaluation of number of overlaps between the singly excited Slater determinants of the KS orbitals (eq 2), which are in turn expressed in terms of localized atomic basis functions.[59] This step was efficiently parallelized in our implementation. The hopping probabilities, $P_{j\to k}$, are calculated on the time scale of electronic dynamics;[55,59,67]

$$P_{j\to k}(t) = -2\Delta\tau \frac{\mathrm{Re}(C_k^*(t)C_j(t)D_{kj}(\mathbf{R}(t)))}{C_j^*(t)C_j(t)} \tag{3}$$

where $\Delta\tau = \Delta t/N$ and $N$ = 2500.

The NA-TDDFT simulations were based on the hybrid version of the 1996 functional of Perdew, Burke, and Ernzerhof (PBE), designated PBE0,[68−70] which combines 75% of Slater + PBE and 25% of HF exchange and Perdew−Wang + PBE correlation. The PBE0 functional was shown to be rather reliable for calculations on the excited states.[67] The Dunning's cc-pVDZ basis set[71] was used, which is expected to be sufficiently accurate provided low-lying valence states are of interest.[72] The initial nuclear positions and momenta were randomly sampled from a preliminary ground state trajectory and correspond to a temperature of 298 K, which although higher than those pertinent to the present experiments was chosen to speed up the dynamics and to incite the occurrence of interesting relaxation phenomena over a reasonable time period. Furthermore, since the TDDFT excited states are grouped much more densely than the RI-CC2 ones (*vide infra*), this additionally facilitated switches between the surfaces. The velocity Verlet algorithm[73] with a time step of $\Delta t$ = 0.25 fs was used to integrate the nuclear equations of motion. The NA-TDDFT trajectories were propagated in a subspace spanned by the ground and four lowest excited electronic states. All trajectories were initiated from the first excited state of the $\gamma_L$(g+) conformer and followed for 5000 steps corresponding to 1250 fs. Our implementation of the NA-TDDFT program is coupled to the TURBOMOLE 6.3 quantum chemistry suite,[74,75] which was also employed for the RI-CC2 calculations.

*2.2.2. Investigation of the Nonradiative Deactivation Paths via Coupled Cluster Calculations.* For the four lowest energy conformers of NAPA, the dominant NRD pathways encountered in the NA-TDDFT simulations have been reinvestigated using the coupled cluster method to the second order (CC2)[76] as a more reliable method.[43,46,77] The resolution of identity (RI) approximation in parallel implementation was used to achieve a faster evaluation of the electron repulsion integrals.[78,79] To make the RI-CC2 calculations affordable, Dunning's cc-pVDZ basis set was employed.[71]

To check for the existence of the CIs along the indicated NRD pathways and to estimate the corresponding RI-CC2/cc-pVDZ barriers, we adopted the following strategies: (i) We make use of constrained optimizations during which all the internal coordinates are allowed to relax apart from the driving coordinate; that is, the one relevant to the NRD processes considered, normally a bond length, which is kept fixed at regular intervals. Such optimizations are expected to approximate well the NRD minimum energy path provided the changes in the relaxing coordinates are minor, which justifies the assumption of their instantaneous response.[80] In critical regions, these constrained optimizations may result in abrupt relocations of the structure to distant regions of the conformational space. When this happens, (ii) we turn to single point calculations at a series of intermediate geometries generated by linearly interpolating the internal coordinates between the last successfully optimized initial and final geometry. In this manner, we adequately cover the critical regions where enforcing a constrained optimization becomes physically unjustified and again deem the thus generated linearly interpolated paths (LIP) to be sufficiently close to the minimum energy NRD paths. The LIP-type calculations were also used to estimate the barriers for interconversion between geometrically distant local minima. (iii) The third strategy consists of fully unconstrained optimizations initiated in regions where a change in the sign of the force corresponding to the driving coordinate from attractive to repulsive is observed. Such a full optimization usually rapidly leads toward regions where the energy difference between two states of interest becomes negligibly small, which is then taken as the confirmation of the CI between them.

## 3. RESULTS

**3.1. Experiment.** The UV spectrum of NAPA, as obtained using R2PI or LIF, has been already published.[49] From IR/UV double resonance spectroscopy, the spectrum (Figure 2) has been shown to be due to three band systems and assigned to three conformers labeled A, B, and C, respectively,

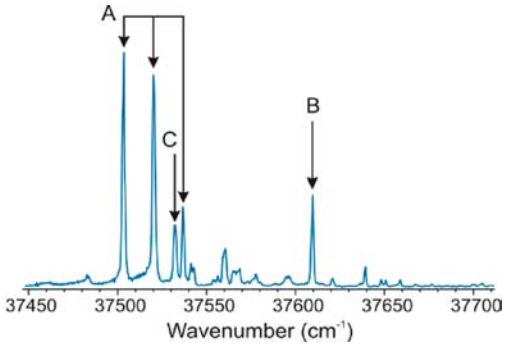


**Figure 2.** R2PI spectrum of NAPA in the region of the origin band of the first $\pi\pi^*$ transition of the phenyl ring, showing the main contributions of three conformers (minor bands are due to A and NAPA hydrates[81]).

unambiguously identified from IR spectra as the $\beta_L$(a), $\gamma_L$(g+), and $\gamma_L$(g−) most stable forms discussed above.[49]

R2PI and LIF yield similar spectra apart from the B band previously not observed in LIF.[33,49,50] A new LIF spectrum (not shown) carried out at a higher sensitivity, namely, using a Nd:YAG pump for the dye laser, enabled us to detect a weak short-lived fluorescence from the B band. A first pump−probe R2PI experiment carried out in the picosecond regime enabled us to measure the lifetime of the excited state of conformer B at the origin band of the first $\pi\pi^*$ transition at 37609 cm$^{-1}$ (Figure 3). The decay obtained (1.5 ± 0.3 ns), consistent with

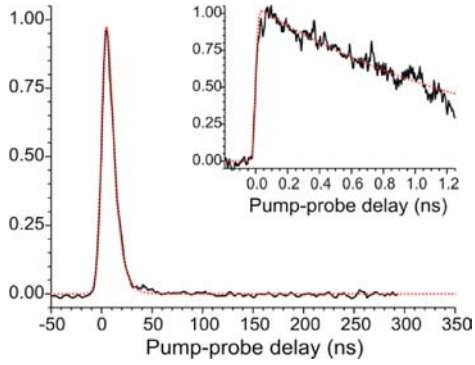


**Figure 3.** Pump−probe signal obtained after pumping the origin transition of NAPA B ($d_0$), with nanosecond lasers and in the inset at a picosecond time scale. The probe laser was tuned to 37400 cm$^{-1}$ (nanosecond) or 36100 cm$^{-1}$ (picosecond). Best fits of the picosecond pump−probe decay provides a lifetime of 1.5 ± 0.3 ns. The nanosecond decay essentially corresponds to the apparatus function.

the observation of a weak fluorescence, is much shorter than the 40−70 ns lifetime range measured for the other conformers, the 86.4 ns lifetime of toluene (the chromophore of NAPA) at its origin[65] (essentially shortened by ISC, quantum yield ∼0.7[61]), and the purely radiative lifetime of toluene (∼250 ns, as estimated from the origin fluorescence lifetime and fluorescence quantum yield, ∼0.30[62]).

Nanosecond pump−probe carried-out on A and C origins confirmed the lifetime values obtained from fluorescence measurements (Table 1), demonstrating that the pump−probe experiment measures the lifetime of the originally photoexcited state. Additional nanosecond measurements carried out by pumping the $6b_0^1$ vibronic transition led to

**Table 1. Excited State Lifetimes (in ns) of Selected Isotopomers of NAPA Measured on the Origin of the $\pi\pi^*$ Transition by LIF or R2PI**

| | species | | conf. A | conf. B | conf. C |
|---|---|---|---|---|---|
| $d_0$ | $NH/NH_2$ | R2PI ps/ns | 70 ± 2 | 1.5 ± 0.3[a] | 35 ± 2 |
| | | LIF | 69 ± 2 | | 38 ± 4 |
| $d_1$ | NH/NHD | R2PI ns | | <3 | |
| | $ND/NH_2$ | | | <3 | |
| $d_2$ | $NH/ND_2$ | R2PI ns | | <3 | |
| | ND/NHD | | | | |
| $d_3$ | $ND/ND_2$ | R2PI ns | 78 ± 2 | <3 | 44 ± 2 |

[a]Picosecond pump−probe experiment.

very similar lifetimes, including the specifically short lifetime for B (see Supporting Information).

The effect of deuteration on the excited lifetime has been studied at the nanosecond time scale from measurements on various isotopologues (see Supporting Information) of the three conformers. The time decays obtained for B as a function of the isotopologue/isotopomer are shown in Figure 4. The

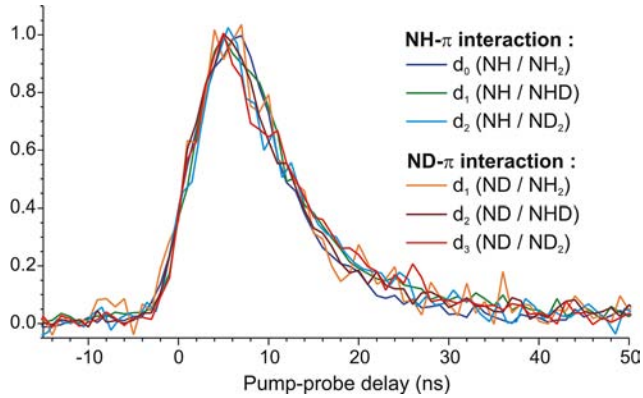


**Figure 4.** Nanosecond pump−probe signals obtained after pumping the origin transitions of several isotopologues (described according to the D content of the NH and $NH_2$ groups) of the B conformer of NAPA ($d_0$−$d_3$). These decays show that deuteration on the NH−$\pi$ interaction site does not affect significantly the excited state lifetime. Fits of the decays are given in Supporting Information. The probe laser was tuned to 37400 cm$^{-1}$.

corresponding best-fit lifetimes are gathered in Table 1. Basically, for conformers A and C, for which only $d_0$ and $d_3$ isotopologues were measured (because of a poor spectral selectivity between the several isotopomers of $d_1$ and $d_2$), a weak deuteration effect on the lifetime is observed. For conformer B, it was spectrally possible with nanosecond lasers to distinguish isotopomers having NH−$\pi$ and ND−$\pi$ H-bonds. For all the $d_0$−$d_3$ species studied (Figure 4), a short lifetime was measured, with an experimental decay signal basically corresponding to the apparatus function (see Supporting Information). An upper limit of the lifetime was estimated to be 3 ns. This absence of a marked deuteration effect, especially the lack of difference between the NH−$\pi$ and ND−$\pi$ conformers, suggests that the $N_{Phe}H$ moiety is not directly involved in the NRD process of conformer B.

**3.2. Nature and Energetics of the Excited States.** In the ground state minimum geometry of all four conformers, the first RI-CC2 excited state is of the $\pi\pi^*$ type, restricted to the phenyl ring chromophore, and derived from the $^1B_{2u}$ state of


dx.doi.org/10.1021/ja3054942 | J. Am. Chem. Soc. 2012, 134, 20340−20351

**Table 2. Vertical, Adiabatic (in parentheses), and ZPE-Corrected Adiabatic (in parentheses, boldface) Excitation Energies (eV) for the Three Lowest Electronic States of $\beta_L$(a), $\gamma_L$(g+), $\gamma_L$(g−), and $\gamma_L$(a) of the Four NAPA Conformers Compared with Adiabatic Experimental Values[a]**

| conformer | RI-CC2/TZVP | RI-CC2/cc-pVDZ | PBE0/cc-pVDZ | expt (present work) |
|---|---|---|---|---|
| $\beta_L$(a) conf. A | 5.163 (4.785) (**4.571**) | 5.252 (4.801) (**4.587**) | 5.368 (5.049) | **4.650** |
| | 5.799 | 5.868 | 5.570 | |
| | 5.841 | 5.962 | 5.697 | |
| $\gamma_L$(g+) conf. B | 5.179 (4.822) (**4.605**) | 5.273 (4.830) (**4.613**) | 5.393 (−) | **4.663** |
| | 5.578 | 5.723 | 5.487 | |
| | 5.817 | 5.874 | 5.674 | |
| $\gamma_L$(g−) conf. C | 5.167 (4.807) (**4.597**) | 5.261 (4.810) (**4.600**) | 5.406 (−) | **4.654** |
| | 5.652 | 5.784 | 5.530 | |
| | 5.883 | 5.949 | 5.629 | |
| $\gamma_L$(a) | 5.191 (4.838) | 5.252 (4.835) | 5.368 (5.181) | |
| | 5.607 | 5.868 | 5.571 | |
| | 5.834 | 5.962 | 5.697 | |

[a]ZPE corrections are based on MP2/cc-pVDZ ground state and RI-CC2/cc-pVDZ excited state harmonic frequencies.

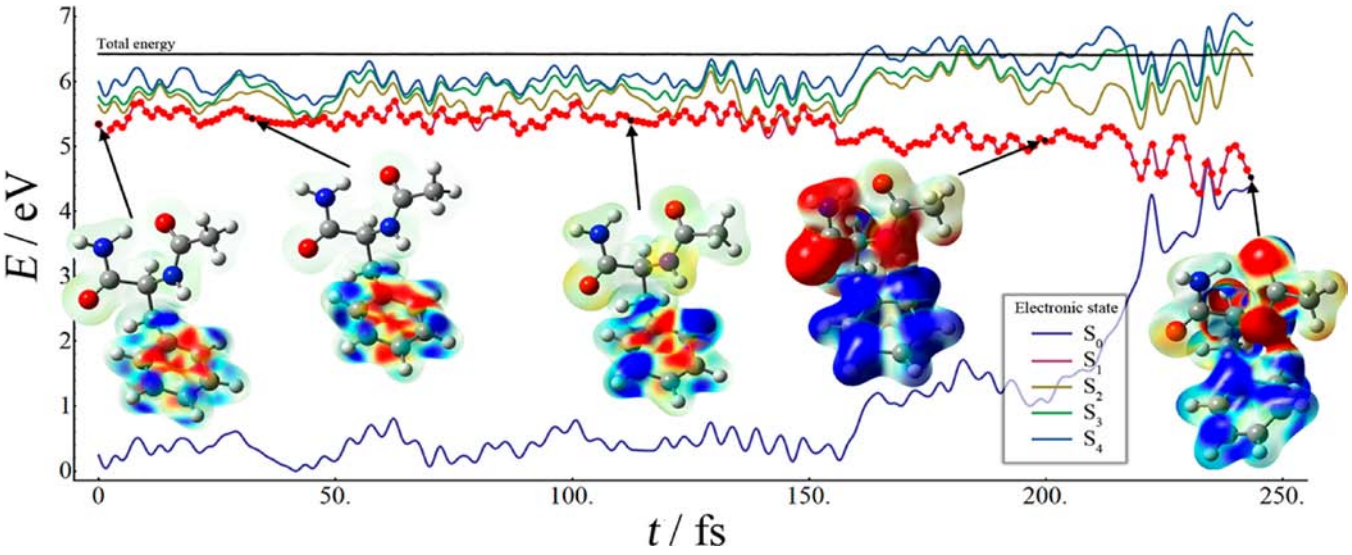


**Figure 5.** Illustration of mechanism I: Time dependence of the potential energy of the ground (blue) and four lowest excited electronic states of $\gamma_L$(g+) along a selected nonadiabatic trajectory. The electronic state in which the trajectory resides is marked with red dots. The nonradiative deactivation to the ground state takes place via H-transfer to the phenyl ring. The insets show the electron density difference of the $S_1$ and $S_0$ states and illustrate the change in the $S_1$ character from $\pi\pi^*$ to CT occurring at around 150 fs. The areas of increased (reduced) electron densities are shown in blue (red). The CI with $S_0$ is reached at around 250 fs. The computations have been performed at the TDPBE0/cc-pVDZ level.

benzene. The next two states are of the $^1n\pi^*$ type localized on the peptide backbone with dominant contributions from an electron density transfer from the oxygen and nitrogen lone pairs to the two carbonyl antibonding orbitals. The fourth is again another state localized on the phenyl ring, analogous to the $^1B_{1u}$ state of benzene. For all four conformers, it is possible to optimize the RI-CC2 $S_1$ minima with only minor geometry changes compared with the corresponding ground states implying that the key conformational features are retained. Table 2 summarizes the CC2 and TDPBE0 excitation energies for the first three excited states of the four NAPA conformers considered. The RI-CC2 adiabatic excitation energies, corrected for zero-point vibrational energy (ZPE), obtained using both the larger TZVP and the smaller cc-pVDZ basis set turn out encouragingly accurate, falling within 0.1 eV of the experimental values (Table 2). Considering that not much accuracy is gained by employing the larger TZVP basis, we opted for the RI-CC2/cc-pVDZ method in characterizing the excited state surfaces, knowing it provides a very good compromise between accuracy and efficiency.

TDDFT yields vertical excitation energies blue-shifted by 0.12−0.15 eV relative to the RI-CC2/cc-pVDZ ones. In agreement with RI-CC2, the lowest-lying ($S_1$) state is predominantly of $\pi\pi^*$ character, localized on the phenyl ring. However, TDPBE0 groups the higher excited states more densely than RI-CC2; moreover, these states are now mixed and hence more difficult to classify because they exhibit various contributions from the ring-localized $\pi\pi^*$ and backbone-localized $n\pi^*$, as well as excitations characterized by a backbone to ring charge transfer. Interestingly, in $\gamma_L$(g+) and $\gamma_L$(g−) a stable TDPBE0 minimum cannot be found on the $S_1$ surface, which is due to the spurious mixing between the valence and the charge transfer states, the latter known to be underestimated by the standard DFT exchange−correlation functionals.[82] Namely, in these conformers, $S_1$ optimization leads to a stretch of the $N_{Phe}H$ bond, which eventually transfers the H atom to the phenyl ring, causing the $S_1$ and $S_0$ states to intersect


dx.doi.org/10.1021/ja3054942 | J. Am. Chem. Soc. 2012, 134, 20340−20351

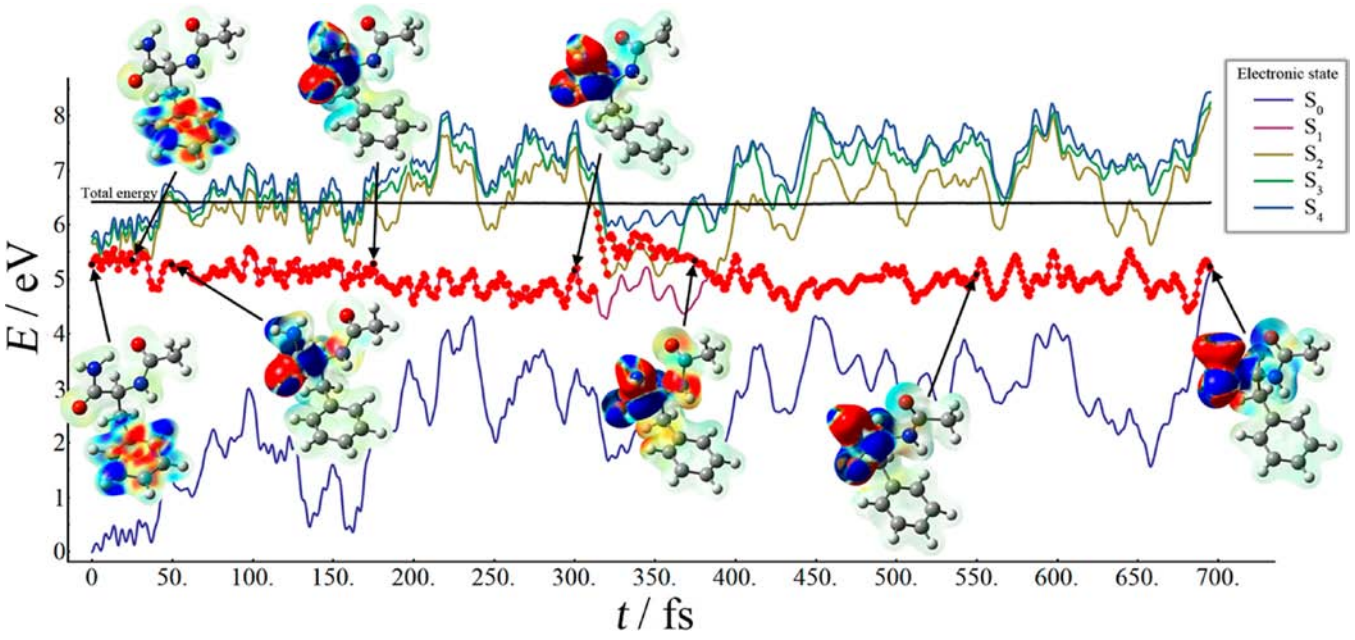


**Figure 6.** Illustration of mechanism II: Time dependence of the potential energy of the ground (blue) and four lowest excited electronic states along a selected nonadiabatic trajectory exhibiting nonradiative deactivation to the ground state via deplanarization of the second peptide bond. See Figure 5 caption for notations. The change in the $S_1$ character at around 60 fs is due to a nonadiabatic transition from the initial $\pi\pi^*$ state to $n\pi^*$ state with excitations localized on the second peptide bond. The CI with the ground state is reached at 700 fs.

and the optimization to crash. This observation already provides hints about one of the possible NRD mechanisms to be discussed later.

**3.3. Nonadiabatic Dynamics Following Photoexcitation.** The NA-TDDFT simulations performed for the $\gamma_L(g+)$ conformer of NAPA, that is, the one with the shortest excited-state lifetime (Table 1), yielded several NRD pathways. Because $\gamma_L(g+)$ exhibits both the principal interactions that govern the conformational features in NAPA, namely, the strong NH···O═C $C_7$ bond and the weaker $N_{Phe}H-\pi$ H-bond, we anticipated that it may display the largest spectrum of NRD mechanisms.

In order to investigate the photodynamics in $\gamma_L(g+)$, we propagated a set of 44 NA-TDDFT trajectories starting from the $S_1$ ($\pi\pi^*$) state, assuming a vertical excitation of ground state conformations. The analysis of the nonadiabatic trajectories suggests that two main types of motions can trigger the NRD mechanisms:

(1) The first one, illustrated by a characteristic trajectory shown in Figure 5, involves a H-transfer from the $N_{Phe}H$ to the C atom in the *ortho* position of the phenyl ring (Figure 1). An analogous transfer to the *ipso* position has also been observed. Figure 5 displays the time variation of the energy of the ground (blue) and four lowest excited electronic states. The insets along the trajectory show the difference in the electronic densities between the current electronic state and $S_0$ on the electron isodensity surface of $S_0$ (isovalue of 0.025/Å$^3$). This changes at ∼150 fs owing to a nonadiabatic transition between the initially excited $\pi\pi^*$ state and a charge transfer state resulting from an electron transfer from the backbone to the phenyl ring. In the selected example, return to the ground state via H-transfer occurs after around 250 fs.

(2) A second type of NRD mechanism involves specific distortions of the backbone geometry occurring either on the first peptide bond or more frequently on the second one (Figure 1). The latter process, involving an apparent deplanarization of the second peptide bond, has a particularly high incidence and was observed in more than half of the NA-TDDFT trajectories. Figure 6 displays a typical trajectory. At the initial geometry, the electronic excitation is localized on the phenyl ring ($\pi\pi^*$ state). Already at 60 fs, one sees a change in the difference of the electron densities indicating a change in the character of the $S_1$ state, from an initial excitation on the phenyl ring to that localized on the second peptide bond and is accompanied by a pyramidalization of N and C atoms of the peptide bond. Specifically, the relaxation mechanism involves a nonadiabatic transition from the initial $\pi\pi^*$ state to a $n\pi^*$ state with excitations localized on the second peptide bond. The loss of planarity of the peptide bond strongly destabilizes the ground state. However, on the basis of the NA-TDDFT simulations alone, it was not possible to unambiguously identify a final NRD mechanism or a reactive coordinate that would promote relaxation to the ground state. In a small fraction of trajectories involving the deplanarization of the first peptide bond, relaxation to the ground state was triggered by H-transfer from the terminal $NH_2$ group toward the locally excited carbonyl O along the H-bond of the $C_7$-ring. Such a process was recently proposed as a viable NRD pathway in similar peptide systems.[19,43−46]

Because the experimental lifetime of the originally excited ($\pi\pi^*$) state is controlled by the access to the *first* CI, we have classified the NRD mechanisms according to the type of the intermediate electronic state populated from the $\pi\pi^*$ state by the first nonradiative transition via the first CI, namely:

(i) Mechanism I, due to the transition from the initial $\pi\pi^*$ state to a charge transfer (CT) state, this latter corresponding to an electron transfer from $\pi$(carbonyl) and nonbonding orbitals of the backbone to the $\pi^*$ orbital of the phenyl ring.

(ii) Mechanisms II and III, due to a transition from the initial $\pi\pi^*$ state to intermediate states, these latter corresponding to backbone excitations (local excitation in the


dx.doi.org/10.1021/ja3054942 | J. Am. Chem. Soc. 2012, 134, 20340−20351

**Table 3. Relative Energies[a] of the Critical Points along the NRD Paths Characterizing Mechanisms I, II, IIIa, IIIb, and IIIc for the Four Conformers of NAPA with Respect to the Corresponding $M_{\pi\pi^*}$ (Adiabatic) Minima[b]**

| | I | II | | | IIIa | | | IIIb | | | IIIc | | |
|---|---|---|---|---|---|---|---|---|---|---|---|---|---|
| conf. | $CI^{I}$ | $CI^{II}$ | $M_{II}$ | $CI^{S0}$ | $CI^{III}$ | $M_{IIIa}$ | $CI^{S0}$ | $CI^{III}$ | $MI_{IIIb}$ | $CI^{S0}$ | $CI^{III}$ | $M_{IIIc}$ | $CI^{S0}$ |
| A $\beta_L$(a) | 0.55 | 0.32 | −0.61 | −0.45 | | | | 0.25 | −0.65 | −0.55 | | | |
| B $\gamma_L$(g+) | 0.48 | 0.22 | −0.71 | −0.52 | 0.36 | −0.78 | −0.63 | 0.26 | −0.69 | −0.60 | 0.23 | −0.72 | −0.60 |
| C $\gamma_L$(g−) | 0.64 | 0.39 | −0.60 | −0.38 | 0.51 | −0.73 | −0.49 | 0.32 | −0.69 | −0.59 | 0.30 | −0.66 | −0.60 |
| $\gamma_L$(a) | | 0.44 | −0.65 | −0.32 | 0.38 | −0.69 | −0.37 | 0.22 | −0.75 | −0.61 | 0.23 | −0.73 | −0.61 |

[a]All values (eV) are given with respect to the conformer's $M_{\pi\pi^*}$ minimum. [b]The following designations are used: conical intersections of the $\pi\pi^*$ and CT ($CI^{I}$); $\pi\pi^*$ and $n\pi^*_{(II)}$ ($CI^{II}$); $\pi\pi^*$ and $n\pi^*_{(III)}$ ($CI^{III}$) states, minima (M), and conical intersection with the ground state ($CI^{S0}$).

terminology of ref 43), more precisely $n\pi^*$ excitations on the second (mechanism II) or the first peptide bond (mechanism III).

The NA-TDDFT dynamics thus pointed to a number of NRD mechanisms to be re-examined at a more accurate level of theory. We commenced by distorting the molecule along the critical coordinates as indicated by the NA dynamics runs.

**3.4. Relaxation Mechanisms.** The CIs between the relevant excited states PES corresponding to the three observed mechanisms were systematically searched for and characterized at the RI-CC2/cc-pVDZ level of theory for the four most stable conformers of NAPA (Table 3). This enables us to propose several NRD pathways illustrated in the following sections, in particular in order to account for the short $S_1$ state lifetime of the $\gamma_L$(g+) conformer. Corresponding details on the relaxation paths of $\beta_L$(a), $\gamma_L$(g−), and $\gamma_L$(a) forms are given in the Supporting Information.

*3.4.1. Mechanism I.* The nonadiabatic trajectory of Figure 5 suggests that mechanism I can be triggered by stretching the $N_{Phe}H$ bond in the direction of the *ortho* C atom of the phenyl ring. Thus, constrained optimizations of the first excited state for a series of fixed $N_{Phe}H$ distances were performed starting from the minimum of the initial $\pi\pi^*$ state, $M_{\pi\pi^*}$. In Figure 7, the potential energy of the ground and four lowest excited states of $\gamma_L$(g+) is plotted against the increasing $N_{Phe}$−H distance. In $\gamma_L$(g+), this elongation gradually disrupts the $\pi$ conjugation pattern of the ring and causes a destabilization of the ground (blue circles) and $\pi\pi^*$ (bordeaux squares) states, whose energy curves exhibit a steep rise in the vicinity of the critical $N_{Phe}$−H distance of 1.2 Å. At around $d(N_{Phe}-H)$ = 1.14 Å, a new state dominated by the charge transfer (CT) excitation from the peptide backbone to the ring emerges in the low-energy spectrum (golden diamonds) and is rapidly stabilized enough to closely approach the $\pi\pi^*$ state (see Figure 7). From $d(N_{Phe}-H)$ = 1.16 Å onward the optimization at fixed $N_{Phe}H$ distances resulted in greatly perturbed structures, which forced us to abandon constrained optimizations. With the further increase in the $N_{Phe}$−H distance, the force between the two atoms becomes repulsive ($d(N_{Phe}-H) \approx 1.22$ Å). Beyond this point, the full geometry optimization confirms a CI with the ground state thus completing the NRD pathway. Thus, to compute the barrier to H-transfer, we constructed a series of LIP geometries by connecting the last meaningful structure from the constrained optimization and the first one for which the forces between the atoms in the $N_{Phe}$−H became repulsive (note the vertical spacers in Figure 7). Following the $S_1$ state along the LIP reveals that the initial clear $\pi\pi^*$ character is gradually altered as contributions of the CT state become more prominent. Around 1.19 Å, a small bump is encountered on the lower surface signifying the minimum in the energy gap between the two states. From here, we estimated the barrier to H-transfer as ∼0.48 eV.

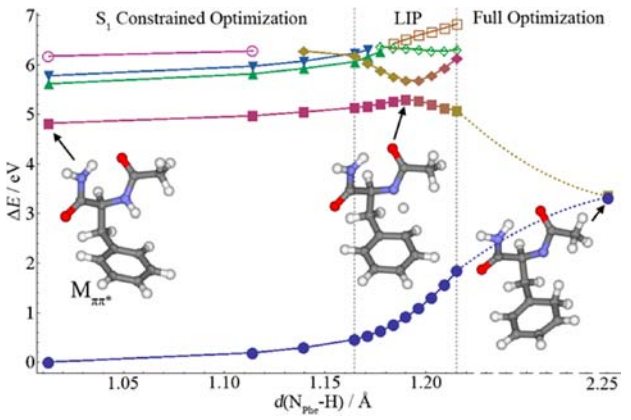


**Figure 7.** Mechanism I: Relative RI-CC2/cc-pVDZ energies of the ground and the four lowest excited states ($\Delta E$) against the $N_{Phe}$−H distance ($d(N_{Phe}-H)$) for the H-transfer from the $N_{Phe}H$ group to the *ortho* C atom of the phenyl ring in the $\gamma_L$(g+) conformer. Vertical delineators indicate different computational strategies (see text): regions of optimizations at fixed $N_{Phe}H$ distances (left), single point calculations on the linearly interpolated path (LIP, middle), and full optimizations (right). The ground state (blue circles), the initial $\pi\pi^*$ state (bordeaux squares), and the final CT state (gold diamonds) are shown together with higher-lying electronic states.

Although no CI is confirmed along the LIP in the strict sense, it has been shown[83] that such minima in gaps are virtually always a hint of a nearby CI ("shoulder of a CI") rather than of an avoided crossing. The elongation of the $N_{Phe}$−H bond leads to the excited state intramolecular H-transfer to the phenyl ring resulting in a cyclohexadienyl intermediate, which is, according to the NBO charges, more accurately described as a diradicaloid, rather than a zwitterion, because the migrating H atom brings some charge to the phenyl ring in the process.

A similar scenario is found for the $\gamma_L$(g−) conformer (see Supporting Information) but here in addition a clear-cut CI between the $\pi\pi^*$ and CT state can be demonstrated. The barrier to the CI, located at practically the same $d(N_{Phe}-H)$ (∼1.20 Å), is appreciably higher than in $\gamma_L$(g+) equaling ∼0.64 eV. That the mechanism I is hampered in $\gamma_L$(g−) compared with $\gamma_L$(g+) is not surprising given that the former lacks the NH−$\pi$ interaction,[37,68−70] which steers the H atom toward the electrophilic addition. The diradical adduct is unstable on the $S_0$ surface, and H is expected to rapidly back-transfer to the $N_{Phe}$ atom.

In the case of $\beta_L$(a), the H addition to the phenyl ring appears also feasible in the first excited state. However, in $\beta_L$(a) the CO−$NH_2$ group, that is, a primary amide, acts as the H donor, and compared with the H-transfer from the secondary


dx.doi.org/10.1021/ja3054942 | J. Am. Chem. Soc. 2012, 134, 20340−20351

(first) amide group, we note an important difference because no approach of a higher state toward the $\pi\pi^*$ state is now seen in the energy profile (Supporting Information). The barrier estimated from the $S_1$ profile is ~0.55 eV.

Overall, mechanism I has the potential to account for relaxation dynamics of the $\pi\pi^*$ excited state in NAPA. It is clearly conformer-dependent because it is not realizable in $\gamma_L$(a) and is furthermore energetically favored in $\gamma_L$(g+) compared with $\gamma_L$(g−), and $\beta_L$(a).

*3.4.2. Mechanism II.* Mechanism II takes place on the NAPA $n\pi^*$ surface characterized by backbone local excitations from the N nonbonding pair to the C═O antibonding $\pi^*$ orbital of the second peptide bond, denoted $n\pi^*$(II). By the frequency of occurrence in the NA-TDDFT simulations, this mechanism represents the most favorable NRD pathway for $\gamma_L$(g+) assuming a vertical excitation. The key to its efficiency is the easily accessible CI between the $\pi\pi^*$ and the $n\pi^*$(II) states. The barrier to the first CI has been calculated by locating first a minimum energy structure, $M_{II}$, on the $n\pi^*$(II) surface and then connecting the two minima, $M_{\pi\pi^*}$ and $M_{II}$, by a series of LIP geometries for which single point energy calculations have been performed. It has to be stressed that $M_{II}$ (as well as $M_{IIIa}$, and $M_{IIIb}$, *vide infra*) has been obtained by a full geometry optimization initiated from structures with a characteristic deplanarization of the second (first) peptide bond such as frequently encountered in the NA-TDDFT simulations. In $\gamma_L$(g+) the $M_{II}$ minimum is found 0.71 eV below the reference $M_{\pi\pi^*}$ minimum. It is distinguished by a marked pyramidalization of the C atom of the second peptide bond, and the O═C—N angles decreased to ~100°, depending on the conformer. Figure 8 illustrates the energy profile for NRD

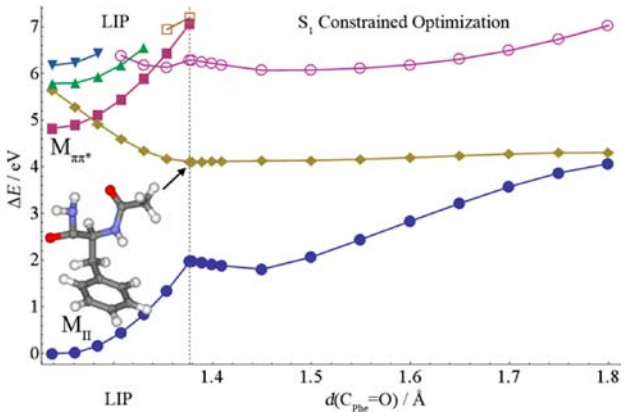


**Figure 8.** Mechanism II: Relative RI-CC2/cc-pVDZ energies of the ground (blue circles) and the four lowest excited states ($\Delta E$) along the LIP involving the readjustment of the peptide backbone from $M_{\pi\pi^*}$ to minimum $M_{II}$ (left), followed by the constrained optimization at fixed C−O distances in $\gamma_L$(g+) (right). The inset shows the $M_{II}$ minimum. See Figure 7 caption for notation.

through mechanisms II in $\gamma_L$(g+) from which it is apparent that the barrier to the first CI lies only 0.22 eV above $M_{\pi\pi^*}$, significantly lower than for the remaining conformers as evident from Table 3.

In order to pinpoint the specific NRD pathway that leads from $M_{II}$ to the CI with the ground state, we made use of the CASSCF optimization and CASPT2 single point calculations on the small auxiliary system acetamide.[20,84] The findings in acetamide proved to be sufficiently transferable to NAPA because it was confirmed that this final CI is most easily approached predominantly through the C═O stretching mode. The NRD pathways are thus verified by a series of constrained optimizations at fixed C−O distances. As apparent from Figure 8, the intersection with the ground state is achieved when the C═O bond is considerably extended, to more than 1.8 Å. We also note a concomitant decrease in the O═C—N angle to ~85°. For $\gamma_L$(g+), the CI with the ground state is found only 0.19 eV above $M_{II}$. Interestingly, the C═O stretch that eventually triggers the approach of the $n\pi^*$ and ground state surfaces is virtually effortless on the $n\pi^*$ surface, while the ground state curve exhibits a typical Morse-like behavior. The latter is still less stiff than what is expected from a double bond, which is a consequence of the greatly deformed $M_{II}$ structure in which the C−O bond is actually closer to a single rather than a double bond. Altogether, mechanism II might indicate the possibility of the C−O bond dissociation accompanied by the release of a singlet oxygen atom.

*3.4.3. Mechanisms III.* The designation III denotes a collection of relaxation mechanisms operational on the $n\pi^*$ surface with dominant excitations located on the first peptide bond, denoted $n\pi^*$(III). On the $\gamma_L$(g+) $n\pi^*$(III) surface, we have located three virtually isoenergetic minima, $M_{IIIa}$, $M_{IIIb}$, and $M_{IIIc}$, with energies of 0.78, 0.69, and 0.72 eV, respectively, below the reference $M_{\pi\pi^*}$ minimum. While $M_{IIIa}$, $M_{IIIb}$, and $M_{IIIc}$ do belong to the same PES, they are found to be separated by comparatively high barriers for interconversion. The following barriers estimated from the LIPs connecting the corresponding minima in $\gamma_L$(g+) were found to amount to 0.77, 0.22, and 0.41 eV for the $M_{IIIa}/M_{IIIb}$, $M_{IIIa}/M_{IIIc}$, and $M_{IIIb}/M_{IIIc}$ cases, respectively. The bottom line is that $M_{IIIa}$, $M_{IIIb}$, and $M_{IIIc}$ are distinct, well-separated minima that are found to relax to the ground state following different pathways. Since the deexcitation pathways from $M_{IIIb}$ and $M_{IIIc}$ are analogous to mechanism II (see Supporting Information), that is, are triggered by the elongation of the C═O bond, here we will detail out only the mechanism IIIa. The relevant energy data for mechanisms IIIa−c are compiled in Table 3.

*3.4.3.1. Mechanism IIIa.* Minimum $M_{IIIa}$ was optimized by adapting the structural features of the previously given "local excitation" (LE) NATMA minimum[44] to NAPA. The CI between the initial $\pi\pi^*$and $n\pi^*$ states was found along the LIP connecting the $M_{\pi\pi^*}$ and $M_{IIIa}$ as shown in Figure 9. It can be reached by overcoming a barrier of ~0.36, 0.51, and 0.38 eV in $\gamma_L$(g+), $\gamma_L$(g−), and $\gamma_L$(a), respectively. From $M_{IIIa}$, the return to the ground state takes place straightforwardly via a second CI found very early along the path of the H-transfer, from the donor $NH_2$ group to the acceptor carbonyl O atom of the first amide, that is, along the $C_7$ H-bond of these folded conformers (Figure 9). The full optimization leads to this CI as soon as the NH bond is only slightly stretched (critical distance of ~1.14 Å). The CI with the ground state lies approximately 0.15, 0.25, and 0.32 eV above the respective $M_{IIIa}$ minima of $\gamma_L$(g+), $\gamma_L$(g−), and $\gamma_L$(a), and is therefore readily accessible from the first CI. Upon switching to the ground state, the migrating H atom is expected to return rapidly to the N donor, as observed in the NA trajectories (see section 3.2).

The barriers to the first CI for the mechanism IIIa are more than 0.1 eV lower than those for mechanism I in case of $\gamma_L$(g+) and $\gamma_L$(g−), where both mechanisms are allowed. Notwithstanding this, the two mechanisms cannot be directly compared solely on basis of the barriers, because I involves a direct H-transfer, while IIIa first involves a deformation of the molecular


dx.doi.org/10.1021/ja3054942 | J. Am. Chem. Soc. 2012, 134, 20340−20351

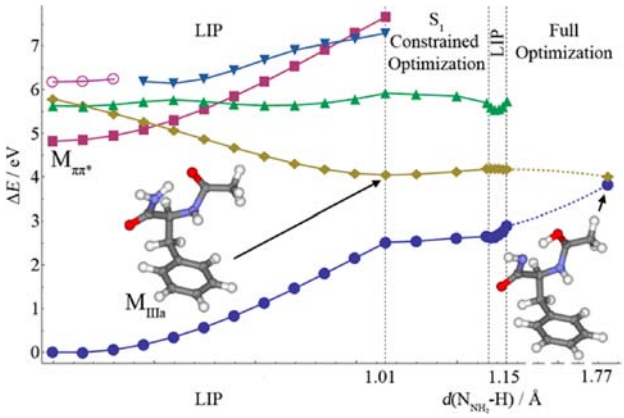


**Figure 9.** Mechanism IIIa: Relative RI-CC2/cc-pVDZ energies of the ground and the four lowest excited states ($\Delta E$) along the LIP from $M_{\pi\pi^*}$ to minimum $M_{IIIa}$ accounting for the readjustment of the peptide backbone (left) followed by optimizations at fixed NH distances for the H-transfer from the $NH_2$ group to the first carbonyl O (middle) and full optimization (right) in the $\gamma_L$(g+) conformer. The three computational strategies are separated by vertical lines. The insets show the $M_{IIIa}$ minimum and the geometry of the conical intersection with the ground state. See Figure 7 caption for notation.

framework and only then the H-transfer. Note in addition that IIIa can be relevant only to the NRD of $\gamma$-conformers.

## 4. DISCUSSION

**4.1. A Large Diversity of Relaxation Pathways.** All the mechanisms suggested by the NA-TDDFT dynamics studies and further verified at the CC2 level of theory (summarized in Table 4) confirm the presence of excited electronic states close to the first optically allowed $\pi\pi^*$ state. In all cases, a distortion of the $\pi\pi^*$ state leads to these secondary states via CIs with relatively low barriers (typically 0.2−0.4 eV). It should be noted that each of the LIP derived barriers represents an upper bound to the true barrier to CI. A way to refine the LIP values would preferably rely on both an automated procedure to locate the minima along a given intersection seam and a multireference method. However, because the former is presently lacking and the latter is unfeasible owing to prohibitively large active spaces to include all the orbitals involved in the NRD mechanisms, the RI-CC2 based LIPs provide a fully acceptable compromise for our present purpose. This point is also evidenced by previous studies employing a similar procedure.[43,45]

Besides the pure electronic barriers to the first CIs, the amount of energy made available by photoexcitation in the reaction coordinate has to be taken into account when considering the capability of the excited state system to cross the barrier and undergo electronic relaxation. This extra energy is the zero point vibrational energy along the reaction coordinate for an adiabatic transition (excitation at the band origin, like in the present experiment) as well as, for example, in the case of a vertical excitation, the vibrational excitation due to the structural difference between ground and excited states minima (see the difference between adiabatic and vertical electronic energies in Table 1), eventually followed by intramolecular vibrational energy redistribution. These arguments make several of the proposed mechanisms possibly responsible for the NAPA deactivation pathways, at least as efficient quenchers of the $\pi\pi^*$ state fluorescence.

The processes presented here bear some resemblance to previously discussed NRD pathways but also have many specific features. Mechanism I is formally similar to the transitions to the $\pi\sigma^*$ state within the SDDJ model[8] to account for the H atom transfer in the excited state of proton donor−acceptor systems or the H ejection of excited state phenol.[85,86] In the present case, the role of the $\sigma^*$ orbital is played by the $\pi_{Phe}^*$ orbital, which leads to an H atom addition to the ring and the formation of a diradical. While excited state H-transfer from the hydroxyl group to the carbon atom of the phenyl ring is known from organic photochemistry,[87] reports on the amide group acting as a proton donor are few. On the experimental side, such a mechanism has long been proposed to interpret the efficient H/D exchange on the 4-position of the tryptophan indole ring in aqueous solution.[88] In the isolated molecule, mechanisms based on H atom transfer have also been recently invoked in the context of NRD of zwitterionic isolated tryptophan,[9] although, in this case, the mechanistic details are quite different (adiabatic sequential proton and electron transfer from the protonated amino group to the indole chromophore). This mechanism has also been indirectly evidenced in free protonated tryptophan ions.[16] The observation of a $m/z$ = 132 fragment after electronic excitation, which corresponds to a $C_\alpha$−$C_\beta$ bond rupture and the presence of two hydrogen atoms on the indolic fragment, was rationalized by an H atom transfer from the protonated amino group to the indole ring during the excited state dynamics.

Mechanism IIIa is reminiscent of the NRD pathway in peptides proposed by Shemesh et al.[43,45] It involves an LE backbone state; however, contrary to the original proposition, it is simpler since it does not necessarily require an additional intersection with a CT state to make its way to the ground state via H-transfer along the $C_7$ H-bond. Mechanisms II and IIIb,c also proceed through a LE state but do not involve H atom

**Table 4. Summary of the Relaxation Mechanisms Suggested by Calculations within the Singlet Multiplicity, Classified According to the First Step, The Second Step, Possible Further Evolution and the Conformer Concerned, Together with Their Corresponding Reaction Coordinates[a]**

| mechanism | 1st nonrad transition (reaction coord.) | 2nd nonrad transition (reaction coord.) | possible further evolution | conformer concerned |
|---|---|---|---|---|
| I | $\pi_{Phe}\pi_{Phe}^* \rightarrow (n_{bb}/\pi_{CO})\pi_{Phe}^*$ ($N_{Phe}H$ distance) (NH distance in $NH_2$) | $(n_{bb}/\pi_{CO})\pi_{Phe}^* \rightarrow$ GS (H atom transfer to the Phe ring) | back transfer of H atom from the Phe ring to the N atom | $\gamma_L$(g+), and to a lesser extent $\gamma_L$(g−) and $\beta_L$(a) |
| II | $\pi_{Phe}\pi_{Phe}^* \rightarrow n_{bb}\pi^*_{CO}$ (2nd peptide bond distortions) | $n_{bb}\pi^*_{CO} \rightarrow$ GS (2nd peptide bond C−O stretch) | 2nd peptide bond C−O relaxation or dissociation | all conformers |
| IIIa | $\pi_{Phe}\pi_{Phe}^* \rightarrow n_{bb}\pi^*_{CO}$ (1st peptide bond distortions) | $n_{bb}\pi^*_{CO} \rightarrow$ GS (H atom transfer from $NH_2$ to CO along the $C_7$ bond) | back transfer of H atom from C−O to the NH | $\gamma_L$(g+), $\gamma_L$(g−), and $\gamma_L$(a); requires a $C_7$ H-bond |
| IIIb and IIIc | $\pi_{Phe}\pi_{Phe}^* \rightarrow n_{bb}\pi^*_{CO}$ (1st peptide bond distortions) | $n_{bb}\pi^*_{CO} \rightarrow$ GS (1st peptide bond C−O stretch) | 1st peptide bond C−O relaxation or dissociation | all conformers |

[a]bb = backbone; GS = ground state; Phe = phenyl.


dx.doi.org/10.1021/ja3054942 | J. Am. Chem. Soc. 2012, 134, 20340−20351

transfer. Beyond the first relaxation step, a wide variety of processes is also invoked that enable, through conical intersections, a fast return of the system to its ground state, the excitation energy being converted into vibration (see Table 4). Such processes leading to an ultrashort excited state lifetime were often conjectured for biomolecules, especially in the case of DNA bases,[89,90] to justify the choice of these systems by the living world in order to minimize the impact of the excited state photochemistry following absorption of UV radiation. Besides nondestructive relaxation pathways, the possibility of a C=O bond dissociation accompanied by the release of singlet oxygen atom can also be envisaged (mechanism II, IIIb, and IIIc). Although upon release the kinetic energy of this powerful oxidant species is expected to be low, similar processes could provide clues toward understanding the mechanism of biological aging of proteins.[91] In connection to that, a recent multireference based photodynamics of formamide showed that the C−N and C=O bonds dissociate most often in the course of the NRD.[92]

**4.2. Adiabatic Excitation and Experimental $\pi\pi^*$ Lifetimes at the Origin Band.** The issue of the excited state lifetime at the adiabatic excitation, that is, following excitation of the vibrationless level of the $\pi\pi^*$ state, can also benefit from the theoretical calculations. The observation of lifetimes much shorter than the radiative lifetime (~250 ns) of toluene demonstrates the occurrence of nonradiative processes. Even in toluene, which features an 86.4 ns lifetime at the origin,[65] and in alkyl benzenes,[64] ISC is found to be already at play. In the case of NAPA, however, the observation of a dramatically shorter lifetime for conformer B (by nearly two orders of magnitude compared with toluene) strongly suggests that a qualitatively different nonradiative process is involved (see Supporting Information).

The different lifetimes measured for the vibrationless levels of the three conformers (Table 1) show that no interconversion occurs between them at least at the origin. Similarly, excitation at the origin forbids any intramolecular vibrational energy redistribution process. It is therefore likely that one (or several) of the mechanisms discussed above do account for the lifetime shortenings observed. It should however be noticed that the lifetimes considered remain significantly long and therefore that the coupling between states is expected to be small. In the case of a vibrationless level, access of the system to the critical region close to the CI can be naively seen as due to the extension of the vibrational wave function of the system in this region. Within such a picture, vibrational modes close to the reaction coordinate will be inasmuch effective for approaching the CI as their zero-point vibrational energy will help accessing the barrier. This should be particularly significant in the case of mechanism I, which exhibits the highest barrier, but benefits in contrast from the large zero-point motion (~0.21 eV) of the NH stretch modes. This consideration enables us to anticipate a significant tunneling to cross the barrier, similarly to what was suggested in the case of phenol,[85,86] where a 0.5 eV excess energy is required to reach the $\pi\pi^*/\pi\sigma^*$ CI from the $\pi\pi^*$ well bottom (lifetime 2.2 ns[85]). The absence of any significant deuteration effect in the lifetime of the three conformers, in contrast to the phenol case for which deuteration changes the excited lifetime by one order of magnitude,[85,86] suggests that mechanism I is not chiefly responsible for the NRD observed.

On this basis, we tentatively assign the dramatic shortening of the experimental lifetime of B to one of the other mechanisms involving a peptide backbone distortion as a primary step, that is II or III. This assignment is supported by the fact that conformer B $\gamma_L$(g+) is theoretically found to exhibit among the lowest barriers for mechanisms II and III (see Table 3). As a matter of fact, the short lifetime features is probably not connected to the presence of the NH−$\pi$ H-bond in this conformer but rather to an orientation of the phenylalanine side chain relative to the backbone more favorable to excitation transfer.

Conformer C $\gamma$(g−) exhibits higher calculated barriers for mechanisms II−III compared with B (Table 3), in agreement with its much longer lifetime: the different phenylalanine side chain orientation could make more difficult the initial excitation transfer from the phenylalanine $\pi$ system to the backbone. One has to mention that, owing to the intermediate time scale reached (~40 ns), mechanisms II or III also compete with ISC for the control of the excited state dynamics.

In the extended conformer A, no significant lifetime shortening nor deuteration effect is observed, suggesting that in addition to the already reduced number of relaxation mechanisms applicable to A, none of them is operative at the origin of the excited state. As in the case of toluene, which has a comparable lifetime,[61,65] ISC is probably the main mechanism responsible for the very slow dynamics observed.

## 5. CONCLUSION

The present paper emphasizes the existence of low-lying excited states of a peptide backbone and suggests they could play an active role in the nonradiative deactivation processes taking place after optical excitation of the phenylalanine residue in neutral peptide chains and more generally in proteins. The theoretical approach strongly lends support to the idea that several types of NRD mechanisms can take place in the excited state after a vertical excitation, all involving local electronic excitations of the backbone moieties and triggered by specific motions of the backbone (NH stretch, peptide bond distortions). It also emphasizes that these processes are expected to be sensitive to backbone environment of the phenyl ring, and therefore, in a more general context, to the phenylalanine residue environment in a protein. This conclusion is supported by experimental results on the excited lifetime of isolated conformers of the model peptide chain NAPA, which also provide evidence for pronounced conformer-specific nonradiative processes in the excited state. In particular, the dramatically shortened lifetime observed in one of the conformers is consistent with two of the NRD mechanisms theoretically found, mechanisms II or III, which proceed through excitations and concomitant deplanarization of the peptide bonds of the molecule. These theoretical predictions suggest new experimental investigations of these isolated systems, for instance, using dedicated pump−probe experiments to measure directly the lifetimes of the excited states at higher excitations and to probe directly the nature of the intermediate states using, for example, a photoelectron detection. The nature of the final products could be probed as well, for instance, by detecting the eventual O atom product of mechanisms II and III, similarly to the detection of the H atom in the dissociation of photoexcited phenol[86] or of larger fragments in the photodissociation of phenylalanine-related compounds.[66]

Besides this important point from the perspective of peptide and protein excited state reactivity, the present results also draw attention to probable experimental pitfalls due to these strongly conformation-dependent lifetimes observed. In particular, gas

phase physical chemists, who often rely on nanosecond experiments to carry out conformational analysis from the conformationally resolved UV spectra, should be aware of this point. Already dramatically present in the UV spectroscopy of isolated DNA bases,[93] this phenomenon seems also to potentially threaten the UV spectroscopy of peptides.

Finally, the present theoretical strategy, based on the combination of nonadiabatic dynamics and a detailed subsequent inspection of the potential energy surfaces using a more accurate method proved fruitful in determining the critical molecular motions that control the NRD pathways. As such, it holds promise for future planned studies on systems as complex as larger peptide chains or hydrates of biomolecules.

## ■ ASSOCIATED CONTENT

### Supporting Information

Appendix S1, experimental details; Appendices S2 and S3, UV and IR/UV spectroscopy of the $d_0$, $d_1$, and $d_2$ isotopologues of NAPA; Appendix S4, considerations on the role of triplet states; Appendix S5, geometries of the optimized stationary points and of the conical intersections found; and figures illustrating the deactivation pathways through the several mechanisms for the $\beta_L$(a), $\gamma_L$(g−), and $\gamma_L$(a) conformers. This material is available free of charge via the Internet at http://pubs.acs.org.

## ■ AUTHOR INFORMATION


### Corresponding Author

iljubic@irb.hr; michel.mons@cea.fr

### Present Addresses

[†]School of Chemical Sciences, National Institute of Science Education and Research, Institute of Physics Campus, PO: Sainik School, Bhubaneswar, Orissa -751 005, India.

[∞]Université Aix-Marseille, CNRS, PIIM UMR 7345, 13397 Marseille cedex 20, France.

### Author Contributions

[‡]M.M. and Y.L. contributed equally to the work.


### Notes

The authors declare no competing financial interest.

## ■ ACKNOWLEDGMENTS

We wish to thank one of the reviewers for relevant remarks on the nanosecond experiment. We acknowledge financial support or contribution from the French-Croatian (Project "Excited States of Peptides in the Gas Phase"; Program Cogito, Hubert Curien partnership), the MZOŠ (Project Numbers 098-0352851-2921 and 098-0982915-2944), the French National Research Agency (Grants ANR-08-BLAN-0158-01 and NT05-1 44224), the "Triangle de la Physique" Foundation (Grants 2008-053T-SERPEBIO and 2010-003T-COMOVA), the GMPCS cluster facility of LUMAT (Orsay), and the Croatian National Grid Infrastructure. N.D. acknowledges the financial support from the Humboldt foundation and would like to thank Prof. V. Bonačić-Koutecký for the stimulating introduction to the field of nonadiabatic dynamics. Fruitful discussions with Dr. D. Babić and Dr. M. Etinski are gratefully acknowledged.

## ■ REFERENCES


(1) Chen, Y.; Barkley, M. D. *Biochemistry* **1998**, *37*, 9976−9982.
(2) Callis, P. R.; Liu, T. Q. *J. Phys. Chem. B* **2004**, *108*, 4248−4259.
(3) Lakowicz, J. R. *Principles of Fluorescence Spectroscopy*, 4th ed.; Springer: New York, 2006.
(4) Shizuka, H.; Serizawa, M.; Shimo, T.; Saito, I.; Matsuura, T. *J. Am. Chem. Soc.* **1988**, *110*, 1930−1934.
(5) McMahon, L. P.; Colucci, W. J.; McLaughlin, M. L.; Barkley, M. D. *J. Am. Chem. Soc.* **1992**, *114*, 8442−8448.
(6) Yu, H. T.; Colucci, W. J.; McLaughlin, M. L.; Barkley, M. D. *J. Am. Chem. Soc.* **1992**, *114*, 8449−8454.
(7) Chen, Y.; Liu, B.; Yu, H. T.; Barkley, M. D. *J. Am. Chem. Soc.* **1996**, *118*, 9271−9278.
(8) Sobolewski, A. L.; Domcke, W.; Dedonder-Lardeux, C.; Jouvet, C. *Phys. Chem. Chem. Phys.* **2002**, *4*, 1093−1100.
(9) Blancafort, L.; Gonzalez, D.; Olivucci, M.; Robb, M. A. *J. Am. Chem. Soc.* **2002**, *124*, 6398−6406.
(10) Callis, P. R.; Vivian, J. T. *Chem. Phys. Lett.* **2003**, *369*, 409−414.
(11) Kang, H.; Dedonder-Lardeux, C.; Jouvet, C.; Martrenchard, S.; Grégoire, G.; Desfrançois, C.; Schermann, J. P.; Barat, M.; Fayeton, J. A. *Phys. Chem. Chem. Phys.* **2004**, *6*, 2628−2632.
(12) Nolting, D.; Marian, C.; Weinkauf, R. *Phys. Chem. Chem. Phys.* **2004**, *6*, 2633−2640.
(13) Kang, H.; Jouvet, C.; Dedonder-Lardeux, C.; Martrenchard, S.; Grégoire, G.; Desfrançois, C.; Schermann, J. P.; Barat, M.; Fayeton, J. A. *Phys. Chem. Chem. Phys.* **2005**, *7*, 394−398.
(14) Grégoire, G.; Jouvet, C.; Dedonder, C.; Sobolewski, A. L. *Chem. Phys.* **2006**, *324*, 398−404.
(15) Boyarkin, O. V.; Mercier, S. R.; Kamariotis, A.; Rizzo, T. R. *J. Am. Chem. Soc.* **2006**, *128*, 2816−2817.
(16) Lepére, V.; Lucas, B.; Barat, M.; Fayeton, J. A.; Picard, V. J.; Jouvet, C.; Çarçabal, P.; Nielsen, I.; Dedonder-Lardeux, C.; Grégoire, G.; Fujii, A. *J. Chem. Phys.* **2007**, *127*, 11.
(17) Grégoire, G.; Jouvet, C.; Dedonder, C.; Sobolewski, A. L. *J. Am. Chem. Soc.* **2007**, *129*, 6223−6231.
(18) Stearns, J. A.; Mercier, S.; Seaiby, C.; Guidi, M.; Boyarkin, O. V.; Rizzo, T. R. *J. Am. Chem. Soc.* **2007**, *129*, 11814−11820.
(19) Sobolewski, A. L.; Shemesh, D.; Domcke, W. *J. Phys. Chem. A* **2009**, *113*, 542−550.
(20) Serrano-Andrés, L.; Fulscher, M. P. *J. Am. Chem. Soc.* **1996**, *118*, 12190−12199.
(21) Ruggiero, A. J.; Todd, D. C.; Fleming, G. R. *J. Am. Chem. Soc.* **1990**, *112*, 1003−1014.
(22) Chen, R. F.; Knutson, J. R.; Ziffer, H.; Porter, D. *Biochemistry* **1991**, *30*, 5184−5195.
(23) Rzeska, A.; Stachowiak, K.; Malicka, J.; Lankiewicz, L.; Wiczk, W. *J. Photochem. Photobiol., A* **2000**, *133*, 33−38.
(24) Rzeska, A.; Malicka, J.; Stachowiak, K.; Szymanska, A.; Lankiewicz, L.; Wiczk, W. *J. Photochem. Photobiol., A* **2001**, *140*, 21−26.
(25) Wiczk, W.; Rzeska, A.; Lukomska, J.; Stachowiak, K.; Karolczak, J.; Malicka, J.; Lankiewicz, L. *Chem. Phys. Lett.* **2001**, *341*, 99−106.
(26) Lukomska, J.; Rzeska, A.; Malicka, J.; Wiczk, W. *J. Photochem. Photobiol., A* **2001**, *143*, 135−139.
(27) Mrozek, J.; Rzeska, A.; Guzow, K.; Karolczak, J.; Wiczk, W. *Biophys. Chem.* **2004**, *111*, 105−113.
(28) Levy, D. H. *Annu. Rev. Phys. Chem.* **1980**, *31*, 197−225.
(29) Cable, J. R.; Tubergen, M. J.; Levy, D. H. *J. Am. Chem. Soc.* **1987**, *109*, 6198.
(30) Eftink, M. R.; Jia, Y. W.; Hu, D.; Ghiron, C. A. *J. Phys. Chem.* **1995**, *99*, 5713−5723.
(31) Dian, B. C.; Longarte, A.; Zwier, T. S. *J. Chem. Phys.* **2003**, *118*, 2696−2706.
(32) Rizzo, T. R.; Stearns, J. A.; Boyarkin, O. V. *Int. Rev. Phys. Chem* **2009**, *28*, 481−515.
(33) Chin, W.; Piuzzi, F.; Dimicoli, I.; Mons, M. *Phys. Chem. Chem. Phys.* **2006**, *8*, 1033−1048.
(34) Gerhards, M. Spectroscopy of Neutral Peptides in the Gas Phase: Structure, Reactivity, Mocrosolvation and Molecular Recognition. In *Principles of Mass Spectrometry Applied to Biomolecules*; Laskin, J., Lifshitz, C., Eds.; Wiley & Sons: Hoboken, NJ, 2006; pp 3−62.

(35) Dian, B. C.; Longarte, A.; Zwier, T. S. *Science* **2002**, *296*, 2369−2373.
(36) Šarić, A.; Hrenar, T.; Mališ, M.; Došlić, N. *Phys. Chem. Chem. Phys.* **2010**, *12*, 4678−4685.
(37) Došlić, N.; Kovacević, G.; Ljubić, I. *J. Phys. Chem. A* **2007**, *111*, 8650−8658.
(38) Rizzo, T. R.; Park, Y. D.; Levy, D. H. *J. Chem. Phys.* **1986**, *85*, 6945.
(39) Cable, J. R.; Tubergen, M. J.; Levy, D. H. *J. Am. Chem. Soc.* **1989**, *111*, 9032.
(40) González, L.; Escudero, D.; Serrano-Andrés, L. *ChemPhysChem* **2012**, *13*, 28−51.
(41) Sobolewski, A. L.; Domcke, W. *Phys. Chem. Chem. Phys.* **2010**, *12*, 4897−4898.
(42) Sobolewski, A. L.; Domcke, W. *ChemPhysChem* **2006**, *7*, 561−564.
(43) Shemesh, D.; Sobolewski, A. L.; Domcke, W. *J. Am. Chem. Soc.* **2009**, *131*, 1374−1375.
(44) Shemesh, D.; Sobolewski, A. L.; Domcke, W. *Phys. Chem. Chem. Phys.* **2010**, *12*, 4899−4905.
(45) Shemesh, D.; Domcke, W. *ChemPhysChem* **2011**, *12*, 1833−1840.
(46) Shemesh, D.; Hättig, C.; Domcke, W. *Chem. Phys. Lett.* **2009**, *482*, 38−43.
(47) Mercier, S. R.; Boyarkin, O. V.; Kamariotis, A.; Guglielmi, M.; Tavernelli, I.; Cascella, M.; Rothlisberger, U.; Rizzo, T. R. *J. Am. Chem. Soc.* **2006**, *128*, 16938−16943.
(48) Domcke, W.; Yarkony, D. R.; Köppel, H. *Conical Intersections: Theory, Computation and Experiment*; World Scientific Publishing Company Incorporated: Singapore, 2011.
(49) Chin, W.; Mons, M.; Dognon, J.-P.; Piuzzi, F.; Tardivel, B.; Dimicoli, I. *Phys. Chem. Chem. Phys.* **2004**, *6*, 2700−2709.
(50) Chin, W.; Mons, M.; Dognon, J. P.; Mirasol, R.; Chass, G.; Dimicoli, I.; Piuzzi, F.; Butz, P.; Tardivel, B.; Compagnon, I.; von Helden, G.; Meijer, G. *J. Phys. Chem. A* **2005**, *109*, 5281−5288.
(51) Lee, Y. H.; Jung, J. W.; Kim, B.; Butz, P.; Snoek, L. C.; Kroemer, R. T.; Simons, J. P. *J. Phys. Chem. A* **2004**, *108*, 69−73.
(52) Hashimoto, T.; Takasu, Y.; Yamada, Y.; Ebata, T. *Chem. Phys. Lett.* **2006**, *421*, 227−231.
(53) Craig, C. F.; Duncan, W. R.; Prezhdo, O. V. *Phys. Rev. Lett.* **2005**, *95*, No. 163001.
(54) Doltsinis, N. L.; Marx, D. *Phys. Rev. Lett.* **2002**, *88*, No. 166402.
(55) Tapavicza, E.; Tavernelli, I.; Rothlisberger, U. *Phys. Rev. Lett.* **2007**, *98*, No. 023001.
(56) Tavernelli, I.; Tapavicza, E.; Rothlisberger, U. *J. Chem. Phys.* **2009**, *130*, No. 124107.
(57) Tavernelli, I.; Curchod, B. F.; Rothlisberger, U. *J. Chem. Phys.* **2009**, *131*, No. 196101.
(58) Tavernelli, I.; Curchod, B. F.; Laktionov, A.; Rothlisberger, U. *J. Chem. Phys.* **2010**, *133*, No. 194104.
(59) Mitrić, R.; Werner, U.; Bonačić-Koutecký, V. *J. Chem. Phys.* **2008**, *129*, No. 164118.
(60) Gloaguen, E.; de Courcy, B.; Piquemal, J. P.; Pilmé, J.; Parisel, O.; Pollet, R.; Biswal, H. S.; Piuzzi, F.; Tardivel, B.; Broquier, M.; Mons, M. *J. Am. Chem. Soc.* **2010**, *132*, 11860−11863.
(61) Dietz, T. G.; Duncan, M. A.; Smalley, R. E. *J. Chem. Phys.* **1982**, *76*, 1227−1232.
(62) Burton, C. S.; Noyes, W. A. *J. Chem. Phys.* **1968**, *49*, 1705−1714.
(63) Huang, C. L.; Jiang, J. C.; Lee, Y. T.; Ni, C. K. *J. Chem. Phys.* **2002**, *117*, 7034−7040.
(64) Lohmannsroben, H. G.; Luther, K.; Stuke, M. *J. Phys. Chem.* **1987**, *91*, 3499−3503.
(65) Hickman, C. G.; Gascooke, J. R.; Lawrance, W. D. *J. Chem. Phys.* **1996**, *104*, 4887−4901.
(66) Tseng, C.-M.; Lin, M.-F.; Yang, Y. L.; Ho, Y. C.; Ni, C.-K.; Chang, J.-L. *Phys. Chem. Chem. Phys.* **2010**, *12*, 4989−95.
(67) Tully, J. C. *J. Chem. Phys.* **1990**, *93*, 1061−1071.
(68) Adamo, C.; Barone, V. *J. Chem. Phys.* **1999**, *110*, 6158−6170.
(69) Perdew, J. P.; Burke, K.; Ernzerhof, M. *Phys. Rev. Lett.* **1997**, *78*, 1396−1396.
(70) Perdew, J. P.; Burke, K.; Ernzerhof, M. *Phys. Rev. Lett.* **1996**, *77*, 3865−3868.
(71) Dunning, T. H. *J. Chem. Phys.* **1989**, *90*, 1007−1023.
(72) Ciofini, I.; Adamo, C. *J. Phys. Chem. A* **2007**, *111*, 5549−5556.
(73) Verlet, L. *Phys. Rev.* **1967**, *159*, 98−103.
(74) Ahlrichs, R.; Bar, M.; Haser, M.; Horn, H.; Kolmel, C. *Chem. Phys. Lett.* **1989**, *162*, 165−169.
(75) Turbomole V6.3 2011, a Development of University of Karlsruhe and Forschungszentrum Karlsruhe Gmbh, 1989−2007. TURBOMOLE GmbH.
(76) Christiansen, O.; Koch, H.; Jorgensen, P. *Chem. Phys. Lett.* **1995**, *243*, 409−418.
(77) Schreiber, M.; Silva, M. R. J.; Sauer, S. P. A.; Thiel, W. *J. Chem. Phys.* **2008**, *128*, No. 134110.
(78) Hättig, C.; Hellweg, A.; Kohn, A. *Phys. Chem. Chem. Phys.* **2006**, *8*, 1159−1169.
(79) Hättig, C.; Weigend, F. *J. Chem. Phys.* **2000**, *113*, 5154−5161.
(80) Auer, B.; Fernandez, L. E.; Hammes-Schiffer, S. *J. Am. Chem. Soc.* **2011**, *133*, 8282−92.
(81) Biswal, H. S.; Loquais, Y.; Tardivel, B.; Gloaguen, E.; Mons, M. *J. Am. Chem. Soc.* **2011**, *133*, 3931−3942.
(82) Dreuw, A.; Head-Gordon, M. *J. Am. Chem. Soc.* **2004**, *126*, 4007−4016.
(83) Truhlar, D. G.; Mead, C. A. *Phys. Rev. A* **2003**, *68*, No. 032501.
(84) Hirst, J. D.; Hirst, D. M.; Brooks, C. L. *J. Phys. Chem. A* **1997**, *101*, 4821−4827.
(85) Pino, G. A.; Oldani, A. N.; Marceca, E.; Fujii, M.; Ishiuchi, S. I.; Miyazaki, M.; Broquier, M.; Dedonder, C.; Jouvet, C. *J. Chem. Phys.* **2010**, *133*, No. 124313.
(86) Dixon, R. N.; Oliver, T. A. A.; Ashfold, M. N. R. *J. Chem. Phys.* **2011**, *134*, No. 194303.
(87) Basarić, N.; Došlić, N.; Ivković, J.; Wang, Y.-H.; Mališ, M.; Wan, P. *Chem.—Eur. J.* **2012**, *18*, 10617−10623.
(88) Saito, I.; Sugiyama, H.; Yamamoto, A.; Muramatsu, S.; Matsuura, T. *J. Am. Chem. Soc.* **1984**, *106*, 4286−4287.
(89) Kohler, B. *J. Phys. Chem. Lett.* **2010**, *1*, 2047−2053.
(90) Markovitsi, D.; Gustavsson, T.; Vaya, I. *J. Phys. Chem. Lett.* **2011**, *1*, 3271−3276.
(91) Berlett, B. S.; Stadtman, E. R. *J. Biol. Chem.* **1997**, *272*, 20313−20316.
(92) Antol, I.; Eckert-Maksić, M.; Barbatti, M.; Lischka, H. *J. Chem. Phys.* **2007**, *127*, No. 234303.
(93) Mons, M.; Piuzzi, F.; Dimicoli, I.; Gorb, L.; Leszczynski, J. *J. Phys. Chem. A* **2006**, *110*, 10921−10924.